Available online at www.sciencedirect.com
ScienceDirect
Trans. Nonferrous Met. Soc. China 22(2012) 2226−2232
Transactions of Nonferrous Metals Society of China
www.tnmsc.cn

Finite element analysis of pressure on 2024 aluminum alloy created during restricting expansion-deformation heat-treatment

ZHAO Na, YANG Yan-qing, HAN Ming, LUO Xian, FENG Guang-hai, ZHANG Rong-jun

State Key Laboratory of Solidification Processing, Northwestern Polytechnical University, Xi'an 710072, China

Received 9 September 2011; accepted 13 January 2012

Abstract: Metals heat-treated under high pressure can exhibit different properties. The heat-induced pressure on 2024 aluminum alloy during restricting expansion-deformation heat-treatment was calculated by using the ABAQUS finite element software, and the effects of the mould material properties, such as coefficient of thermal expansion (CTE), elastic modulus and yield strength, on the pressure were discussed. The simulated results show that the relatively uniform heat-induced pressure, approximately 503 MPa at 500 °C, appears on 2024 alloy when 42CrMo steel is as the mould material. The heat-induced pressure increases with decreasing the CTE and the increases of elastic modulus and yield strength of the mould material. The influences of the CTE and elastic modulus on the heat-induced pressure are more notable.

Key words: aluminum alloy; heat-induced pressure; finite element modeling; temperature field; stress field; material properties

1 Introduction

2024 aluminum alloy has been widely used in many fields such as aerospace, automobile and radar, owing to its high strength, small density and excellent heat resistance. For example, it can be applied as the skin, panels, frames, blades, piston, cylinder head and screw in aircraft manufacturing and the liquid fuel tank of rocket [1]. The main means to strengthen the 2024 aluminum alloy focus on the solution treatment and artificial aging, which are generally carried out under the normal pressure conditions, without considering the influence of pressure on microstructure and properties of the material. Since many new phenomena of materials will appear under high pressure, such as new structural phase transition, valence changes and superconductivity changes [2−5], the treatment methods under high temperature and high pressure are increasingly concerned [6].

High pressure devices currently used for experimental studies are diamond anvil and cubic high-pressure device and so on [7]. The devices rely on the external force to produce a local high pressure environment, which makes the devices have no enough cavity. For example, in order to obtain a high pressure in the diamond anvil, the cavity volume is only 10^{-1}–10^{-4} mm^3. It is clear that the device can only be used in micro-structural analysis of samples and unsatisfied for macro-performance test, which directly limits their engineering applications.

Considering the limitation of the current high pressure devices, HAN et al [8] proposed a device of heat-induced pressure, in which a sample material with a larger coefficient of thermal expansion (CTE) was tightly wrapped by mould material with a smaller CTE to restrict the expansion deformation of the sample during heating process, and the pressure can be generated spontaneously on the sample. Based on the idea, a pressure heat-treatment experiment was done to produce certain pressure on an as-extruded 2024 aluminum alloy which was wrapped in 42CrMo mould (2024/mould) [8]. It is shown that no recrystallization of the as-extruded 2024 alloy happens at 500 °C for 2 h, and the 2024 alloy maintains its original elongated grains, indicating that the pressure environment inhibits the recrystallization process of the 2024 alloy, and the microstructure of the treated 2024 alloy is shown in Fig. 1. However, the value of the pressure in the device cannot be directly measured in experiment. Therefore, an effective simulation to

Foundation item: Project (51071125) supported by the National Natural Science Foundation of China; Projects (SKLSP201107, SKLSP 201124) supported by the Fund of the State Key Laboratory of Solidification Processing in Northwestern Polytechnical University, China
Corresponding author: YANG Yan-qing; Tel: +86-29-88460499; E-mail: yqyang@nwpu.edu.cn
DOI: 10.1016/S1003-6326(11)61453-2

characterize the pressure is highly desired.

ABAQUS is one of the most powerful finite element (FE) calculation software, by which many issues including structural analysis and heat transfer problem with its strong nonlinear analysis capability can be simulated. The effectiveness has been verified whether in scientific research or in engineering applications [9]. In this work, ABAQUS FE software was employed to simulate the heat-induced pressure generated during the 2024/mould pressure heat treatment at 500 °C. Furthermore, the influences of CTE, elastic modulus and yield strength of mould material on the pressure were discussed.

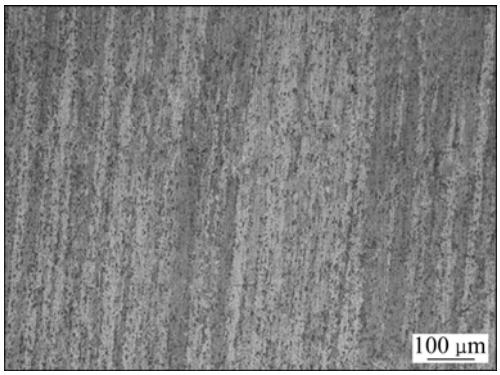

Fig. 1 Microstructure of 2024 aluminum alloy treated in heat-induced pressure device at 500 °C for 2 h

2 Calculation method and model

A sequential thermal-mechanical coupling analysis was carried out in this work. Firstly, a thermal analysis is done, and then the subsequent mechanical analysis is conducted using the temperature histories computed by the thermal analysis as the thermal loading to get the stress and strain fields.

2.1 Basic thermal conduction equations and boundary conditions

For a three-dimensional shape, the thermal conduction equation is as follows:

$$\rho c\frac{\partial T}{\partial t}=\frac{\partial}{\partial x}(\lambda\frac{\partial T}{\partial x})+\frac{\partial}{\partial y}(\lambda\frac{\partial T}{\partial y})+\frac{\partial}{\partial z}(\lambda\frac{\partial T}{\partial z})+q_{\mathrm{v}} \quad (1)$$

where $T(x, y, z, t)$ is the object temperature; ρ is the density; c is the specific heat capacity; λ is the thermal conductivity; t is the time; (x, y, z) is the space coordinates in the objects; and q_{v} is the internal heat source. For the materials involved in this work, both the specific heat capacity and the thermal conductivity have non-linear features, and q_{v} is equal to zero for no heat source inside the material.

In the pressure heat treatment, the 2024/mould was heated to 500 °C by an electric furnace according to actual experimental conditions, and then cooled to room temperature. The heat transfer condition between the outer surface of the device and the ambient temperature belongs to the third boundary condition [10]:

$$\lambda\frac{\partial T}{\partial n}\Big|_{\tau}=h(T_{\mathrm{s}}-T_{\mathrm{q}}) \quad (2)$$

where h is the surface heat transfer coefficient; τ is the heat transfer boundary; T_{s} is the surface temperature; and T_{q} is the ambient temperature.

The heat transfer conditions among the various parts are the fourth boundary condition, namely the heat transfer between solid and solid. It is assumed that different parts are fully contacted, and only the way of heat conduction exists [11].

2.2 Heat-induced pressure−contact pressure

The relationship between the temperature and the strain $\Delta\varepsilon$ caused by temperature change during the heating and cooling processes meets Eq. (3):

$$\Delta\varepsilon=\alpha(T-T_0) \quad (3)$$

where α is the CTE; T_0 is the initial temperature; and T is the real temperature.

Heat-induced pressure at the 2024/mould interface is the so-called contact pressure. The calculation of the pressure can be expressed as [12]:

$$\sigma=D(\varepsilon-\Delta\varepsilon) \quad (4)$$

where σ is the pressure matrix; D is the elastic matrix (related to elastic modulus); ε is the strain matrix; and $\Delta\varepsilon$ is the temperature-induced strain.

Equations (3) and (4) show that the heat-induced pressure can be affected by the elastic modulus, CTE and temperature change. In addition, the stress and strain can be influenced by material strength, so the strength will also have an effect on the heat-induced pressure.

2.3 Finite element model

The schematic diagram of the 2024/mould pressure heat treatment model is shown in Fig. 2(a). The exterior size of the whole is d50 mm × 80 mm, and the diameters of the sample, cylindrical pin, and the mould center hole are 10 mm, 20 mm, and 10 mm, respectively. The sample in Fig. 2(a) is divided into two parts. One is located in the upper and lower side of the center hole and the other is between the two fixed cylindrical pins. Without axial restriction the former can expand freely, while the latter, the object of interest in this work, cannot because its radial expansion is limited by the outer mould and the axial expansion by the two fixed cylindrical pins. A magnitude of 0.02 mm interference fit is adopted among the various parts to realize the sample completely closed.

Because of symmetry as well as for convenience of calculation, only one eighth of the model is used for finite element calculation, as shown in Fig. 2(b). Two simulation element types are used in the model, namely DC3D20 and C3D8R. The DC3D20 is a kind of thermal analysis element used in the thermal analysis and the C3D8R is a kind of structural element used in stress analysis.

In the model, the sample material is 2024 aluminum alloy, and the cylindrical pins and mould are 42CrMo mould material, both of which are treated as work hardening elastic-plastic materials using the Mises yield criterion. The thermal and mechanical properties are shown in Tables 1−3 [13−18].

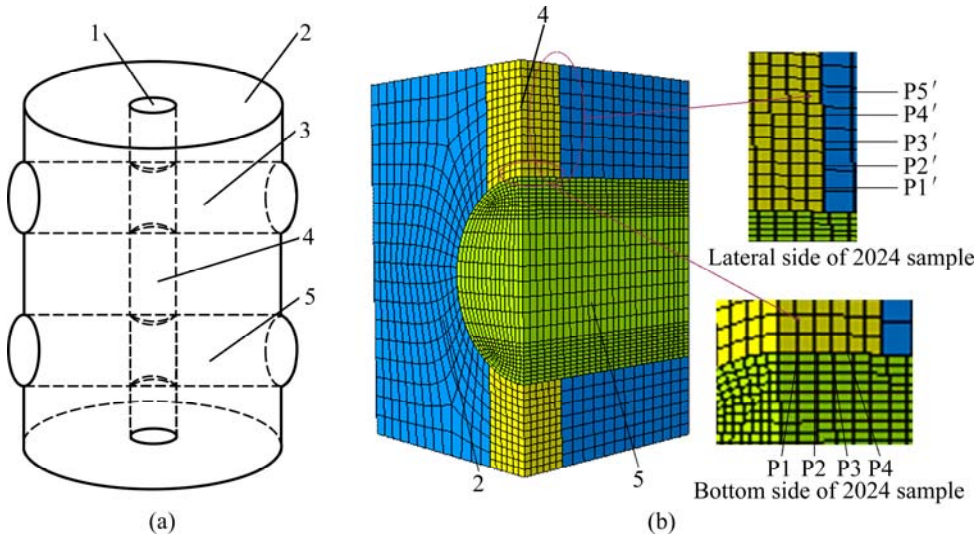

Fig. 2 Schematic drawing of 2024/mould pressure heat treatment model (a) and finite element mesh of model (b): 1—Center hole; 2—42CrMo mould; 3—Upper cylindrical pin (42CrMo); 4—2024 sample; 5—Lower cylindrical pin

Table 1 Thermal and mechanical properties of 2024 aluminum alloy [13−16]

Temperature/ °C	Thermal conductivity/ ($W·m^{-1}·K^{-1}$)	Specific heat capacity/ ($J·kg^{-1}·K^{-1}$)	Elastic modulus/GPa	Poisson ratio	Yield strength/MPa	Density/ ($kg·m^{-3}$)	Thermal expansion coefficient/10^{-6}
20	164	881	72.4	0.33	473.0	2780	14.000
100	182	927	66.5	0.33	416.5	2780	23.018
200	194	1047	63.5	0.33	293.5	2780	24.509
300	202	1130	60.4	0.33	239.8	2780	25.119
400	210	1210	56.1	0.33	150.0	2780	25.594
500	220	1300	50.0	0.33	100.0	2780	26.637

Table 2 Thermal and mechanical properties of 42CrMo steel [17]

Temperature/ °C	Thermal conductivity/ ($W·m^{-1}·K^{-1}$)	Specific heat capacity/ ($J·kg^{-1}·K^{-1}$)	Elastic modulus/GPa	Poisson ratio	Yield strength/MPa	Density/ ($kg·m^{-3}$)	Thermal expansion coefficient/10^{-6}
20	56.0	470	210	0.30	600	7850	7.416
100	52.5	484	205	0.30	570	7850	11.095
200	49.0	521	195	0.30	540	7850	12.445
300	45.5	560	185	0.30	480	7850	13.052
400	42.0	607	175	0.30	400	7850	13.663
500	38.5	668	160	0.30	300	7850	14.084

Table 3 Surface convection coefficient of 42CrMo [18]

Temperature/°C	50	100	200	300	350	400	500
h_c/($W·m^{-2}·°C^{-1}$)	2000	3800	6000	13500	14000	12500	7000

3 FEM results and discussion

3.1 Temperature field analysis

Figure 3 shows the simulated temperature distribution of the pressure model during heating and cooling processes.

The temperature distributes basically uniformly on the whole model at 500°C for 2 h, the value in the heart is slightly lower than that of outer surface and the temperature difference is less than 0.0001 °C. The whole model returns to room temperature after water cooling. At the instant of cooling process from 500 °C, such as, at the 10th second, a great temperature difference exists between the center and the external, and the difference value is up to 330 °C, as shown in Fig. 3(b).

3.2 Heat-induced pressure analysis

The obtained stress and heat-induced pressure fields of various parts at 500 °C are shown in Fig. 4. The heat-induced pressure at the cylindrical pin/sample and sample/mould interfaces is fairly uniform except the corners for shape changes (see Figs. 4(a), (b) and (d)). Heat-induced pressure at the cylindrical pin/sample interface is very large, while the value is comparatively small at the cylindrical pin/mould interface, because the two parts are the same material without difference in CTE. The lateral and bottom sides of the sample are

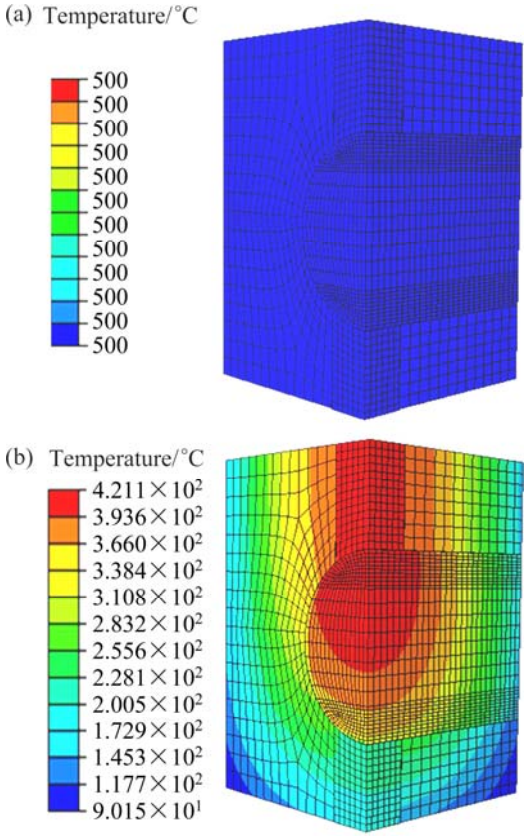

Fig. 3 Temperature distribution of 2024/mould pressure heat-treatment model: (a) Heating up to 500 °C; (b) At the 10th second of cooling process from 500 °C

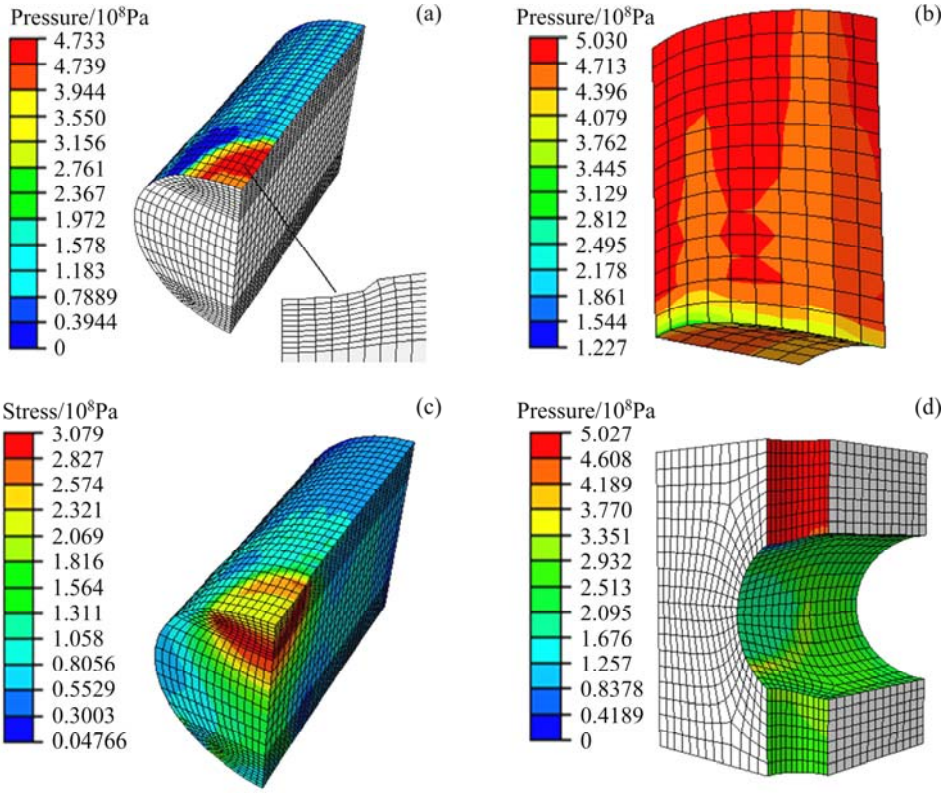

Fig. 4 Distribution of heat-induced pressure and stress: (a) Heat-induced pressure of cylindrical pin; (b) Heat-induced pressure of 2024 alloy; (c) Mises stress of cylindrical pin; (d) Heat-induced pressure of mould

subjected to a more uniform heat-induced pressure, and the value on the bottom is slightly smaller than that of the lateral side, which may be related to the content of shape regulation. The heat-induced pressure is up to 503 MPa at 500 °C when 42CrMo is used as the mould material.

Figure 4(c) indicates that the Mises stress of cylindrical pin is very large and in some regions the Mises stress is larger than the yield strength of 42CrMo. In Fig. 4(a), a certain degree of arc-shaped bending deformation appears in the area of cylindrical pin contacting with the sample, and the maximum deformation is located at the central axis. As the temperature increases, the contact area of cylindrical pin will endure the heat-induced pressure. Furthermore, the ends of the cylindrical pin are restricted by the mould. This case is equivalent to a fixed simple beam resulting in elastic-plastic deformation of the cylindrical pin, which indicates that high heat-induced pressure does exist at the high temperature.

3.3 Influence factors of heat-induced pressure

Based on the above FE analysis, it is known that the properties of the mould material, such as CTE, elastic modulus and yield strength, influence the heat-induced pressure acting on the sample 2024 alloy. Therefore, the controlling variable method, that is, changing one property of the mould material while keeping others invariant, is adopted to study the effect of the properties of the mould material on heat-induced pressure acting on 2024 alloy by FE simulation. As marked in Fig. 2(b), contact points, namely P1, P2, P3, P4 at sample/cylindrical pin interface and P1′, P2′, P3′, P4′, P5′ at sample/mould interface are selected to investigate the effect of the properties of the mould material on heat-induced pressure at 500 °C.

The influence of the CTE change of mould material on heat-induced pressure that acts on the sample 2024 alloy at 500 °C is plotted in Fig. 5. The abscissa of Fig. 5 represents the change of the CTE based on that of 42CrMo normalized as 1. It can be seen that because of the large CTE mismatches between the mould material and sample material, inducing the pressure, the smaller the CTE of the mould material, the larger the heat-induced pressure acting on the sample 2024 alloy. However, the heat-induced pressure on the sample 2024 alloy decreases rapidly with the increase of the CTE of mould material. When the CTE of mould material is 1.5 times that of 42CrMo, nearly no CTE difference exists, resulting in that the pressure is very small and almost close to the interference assemble pressure. When the amplitude scaling factor is 2, the expansion of mould material becomes larger than that of the sample material, which leads to clearance existing at the interfaces and

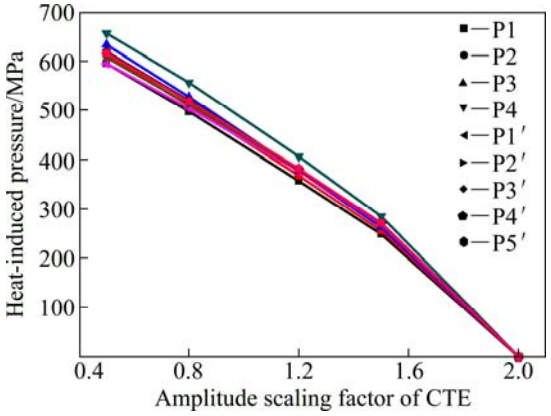

Fig. 5 Influence of CTE on heat-induced pressure

then the interference has no effect. So the heat-induced pressure is almost zero.

Figure 6 shows the change of the heat-induced pressure with changing the elastic modulus of mould material at 500 °C. The heat-induced pressure on the bottom and the lateral sides of sample both rapidly increase as the elastic modulus of mould material increases. It is clear that the elastic modulus reflects the ability of material to resist the elastic deformation. The greater the elastic modulus, the more difficult the mould to deform, leading to a stronger restriction of mould material to the expansion of sample and so the larger heat-induced pressure. It is indicated in Fig. 6 that when the elastic modulus is 100−250 GPa, the heat-induced pressure increases faster, and when increasing the elastic modulus of each 50 GPa, the heat-induced pressure raises by about 100 MPa. Afterwards the increase of the heat-induced pressure becomes slower gradually. The heat-induced pressure increments of only about 50 MPa can be obtained when increasing the elastic modulus of each 50 GPa. The pressure is up to 650 MPa at 500 °C when the elastic modulus reaches 350 GPa.

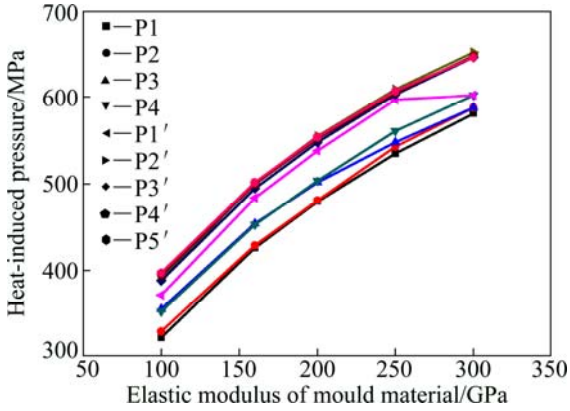

Fig. 6 Influence of elastic modulus on heat-induced pressure

As mentioned above, the plastic deformation of the mould material appears at 500 °C (Fig. 4). Obviously, the

plastic deformation decreases the heat-induced pressure acting on the sample 2024 alloy. As shown in Fig. 7(a), the heat-induced pressure on the bottom and lateral sides of the sample increases gradually with the increase of the yield strength of mould material at 500 °C. It is known that yield strength is the minimum stress for material to be in plastic deformation. It is clear that the larger yield strength of the mould material makes the plastic deformation more difficult and restricts the expansion of the 2024 sample more effectively, which can lead to the larger heat-induced pressure. When the yield strength at 500 °C is 300−600 MPa, the heat-induced pressure on both the bottom and lateral sides of sample grows rapidly as the yield strength increases. And then the growth of the heat-induced pressure slows down gradually, especially the heat-induced pressure on the bottom when the yield strength is larger than 600 MPa.

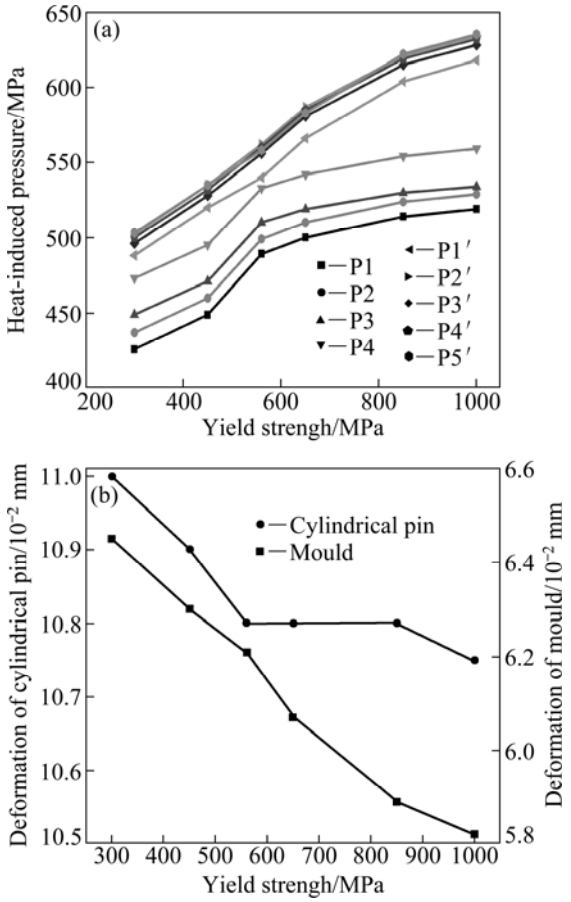

Fig. 7 Influence of yield strength on heat-induced pressure (a) and on plastic deformation (b) of mould and cylindrical pin

It can be seen from Fig. 7(a) that the heat-induced pressure on the bottom is smaller than that on the lateral side. Furthermore, the value on the bottom increases gradually from the center point P1 to the end point P4 of the pin, which is probably due to the irregular intersecting sample/cylindrical pin interface, while the heat-induced pressure on the lateral is comparatively uniform probably because of the regular shape of the lateral side of sample.

Figure 7(b) shows that the plastic deformation of the mould materials takes place although the heat-induced pressure is smaller than the yield strength of the materials. It is known that whether the mould has yielded or not is determined by the Mises stress rather than by the pressure. Figure 8 gives an example of the Mises stress of the mould with yield strength of 1000 MPa. It can be seen that at P5′, the heat-induced pressure is only 630 MPa, but the Mises stress exceeds the yield strength of the mould material, leading to plastic deformation. Figure 7(b) illustrates that the plastic deformation of the pin and the mould decreases with the increase of the yield strength. The different plastic deformation makes the heat-induced pressure different in Fig. 7(a). The plastic deformation of cylindrical pin is significantly larger than that of the mould, resulting in a larger space in the center, which will weaken the restriction to the expansion of sample. This confirms, on the other hand, the fact that the increment of the pressure on the lateral side is larger than that on the bottom, as indicated in Fig. 7(a).

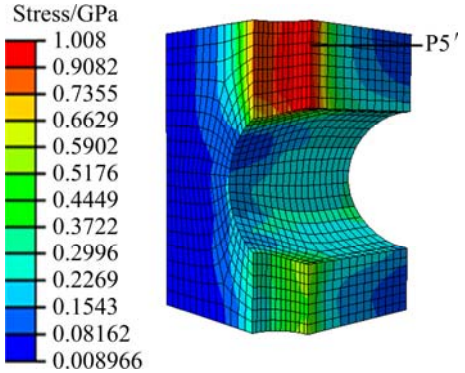

Fig. 8 Mises stress of mould with yield strength of 1 GPa

Comparing the effects of CTE, elastic modulus and yield strength of mould material on the heat-induced pressure acting on the sample 2024 aluminum alloy, it seems that the effects of CTE and elastic modulus are more notable.

4 Conclusions

1) The finite element simulation of the 2024/mould pressure heat treatment indicates that high heat-induced pressure can be generated on 2024 sample, which is approximately 503 MPa at 500 °C when 42CrMo is used as the mould material. Moreover, the pressure distributions on both the bottom and lateral sides are relatively uniform.

2) The heat-induced pressure increases with decreasing the CTE and the increases of elastic modulus

and yield strength of the mould material. Furthermore, the influences of the CTE and elastic modulus on the heat-induced pressure are more notable.

References

[1] LIU Jing-an, XIE Shui-sheng. Application and development of aluminum alloys [M]. Beijing: Metallurgical Industry Press, 2004: 128−129. (in Chinese)

[2] RUBIE D C, BREARLEY A J. Mechanism of the phase transformation of Mg_2SiO_4 at high temperature and pressure [J]. Nature, 1990, 348: 628−631.

[3] SAXENA S K. Science at extreme conditions [J].Science, 1994, 264: 405−407.

[4] SHIMIZU K, KIMURA T, FUROMOTO S, TAKEDA K, KONTANI K. Superconductivity in the non-magnetic state of iron under pressure [J]. Nature, 2001, 412: 316−318.

[5] JEANOLZ R, HAZEN R M. Composition limits of Fe_xO and the earth's lower mantle [J]. Science, 1993, 261: 923−925.

[6] ZHANG Zhen-ning. Effect of high pressure treatment on microstructure and properties of LY12 aluminum alloy [D]. Qinghuangdao: Yanshan University, 2009. (in Chinese)

[7] XIE Hong-sen. Materials science of the earth's interior introduction [M]. Beijing: Science Press, 1997: 11−15. (in Chinese)

[8] HAN Ming, YIN Wen-hong, YU Zhong-hui, KONG Fang-fang, SUN Rui-tao. Heat-induced pressure device with fixed hinge pin: CN 200820021408.7 [P]. (in Chinese)

[9] WANG Jing-chang, CHEN Ye-kai. Application of Abaqus in civil engineering [M]. Hangzhou: Zhejiang University Press, 2006: 1−2. (in Chinese)

[10] YIN Wen, LEI Hong. Numerical simulation of symmetrical workpiece of quenching processes [J]. Journal of Jimei University, 1998, 3(4): 55−59. (in Chinese)

[11] ZHU Shang. Temperature analysis of concrete filled steel tube under high pressure [J]. Architectural and Structural Design, 2006, 5: 36−37. (in Chinese)

[12] ZHU Ai-qiang, LIU Zuo-min. The effect of materials matching on friction temperature field of disc brake [J]. Lubrication Engineering, 2008, 33(3): 62−65.

[13] SHI Q Y, DICKERSON T, SHERCLIFF H R. Thermo-mechanical analysis on welding process of aluminum 2024 with TIG and FSW [C]//Proceedings of the 6th International Conference on Trends in Welding Research. Georgia, USA, 2003: 247−252.

[14] Editorial Committee of Chinese Aeronautical Materials Handbook. Chinese aeronautical materials handbook [M]. 1st ed. Beijing: China Standards Press, 1988: 42−43. (in Chinese)

[15] WANG Chun-kui, LIU Xiao-ping. Dynamic properties of LY12 aluminum alloy under high temperature condensed state-high temperature elastic modulus measurements [J]. Chinese Journal of High Pressure Physics, 1991, 5(1): 33−34. (in Chinese)

[16] WILLIAM F, ROWN J R. Aerospace structural metals handbook [M]. Traverse City, Michigan: Mechanical Properties Data Center, 1975.

[17] YUAN You-lu, ZENG Da-xin, DONG Yi, LIN Yue-jun. Simulation and experimental investigation on investment casting process of complex 42GrMo steel castings [J]. Foundry, 2008, 57(5): 474−476.

[18] LAI Hong, LIU Tian-mo. Temperature filed Ansys simulation in quenching process of 45 steel part [J]. Journal of Chongqing University, 2006, 3(3): 82−83.

2024 铝合金限制膨胀变形热处理产生高压的有限元分析

赵 娜，杨延清，韩 明，罗 贤，冯广海，张荣军

西北工业大学 凝固技术国家重点实验室，西安 710072

摘 要：采用限制热膨胀变形的热处理方法在 2024 铝合金上产生热致压力，利用 ABAQUS 有限元软件模拟计算其热致压力，考察模具材料的热膨胀系数、弹性模量和屈服强度等材料性能对热致压力的影响规律。结果表明：该装置在 500 ℃ 时能够产生比较均匀的热致压力，当模具材料采用 42CrMo 时，热致压力最大可达 503 MPa；热致压力随着模具材料热膨胀系数的减小、弹性模量以及屈服强度的增加而增大，模具材料的热膨胀系数和弹性模量对热致压力的影响更明显。

关键词：铝合金；热致压力；有限元模拟；温度场；应力场；材料性能

(Edited by LI Xiang-qun)